

Performance Evaluation of BICM–OFDM Systems Impaired by UWB Interference

Amir Nasri, Robert Schober, and Lutz Lampe
University of British Columbia, {amirn,rschober,lampe}@ece.ubc.ca

Abstract—In this paper, we propose a theoretical framework for the analysis of the impact of ultra–wideband (UWB) interference on systems that use the popular combination of bit–interleaved coded modulation (BICM) and orthogonal frequency–division multiplexing (OFDM). For the UWB interference we consider multi–band OFDM (MB–OFDM), direct–sequence UWB (DS–UWB), and impulse–radio UWB (IR–UWB) formats following recent IEEE/ECMA standards and standard proposals. Our analysis is applicable to generic BICM–OFDM victim systems including IEEE 802.11 wireless local area networks (WLANs), IEEE 802.16 wireless access systems (WiMAX), and 4th generation mobile communication systems. Besides the exact analysis we also calculate the bit–error rate for the case when the UWB interference is modeled as additional Gaussian noise. Our results show that in general the BER of the BICM–OFDM system strongly depends on the type of the UWB interference and the sub–carrier spacing. While the Gaussian approximation is very accurate for DS–UWB, it may severely over– or underestimate the true BER for MB–OFDM and IR–UWB interference.

I. INTRODUCTION

The performance of licensed narrowband (NB) systems in the presence of ultra–wideband (UWB) interference has been studied extensively in the past few years, cf. e.g. [1]–[6]. Besides mobile communication systems [2], such as the Global System for Mobile Communication (GSM) and the Universal Mobile Telecommunication System (UMTS), and generic uncoded systems [1], [6], wireless local area networks (WLANs) [3], [4] and fixed wireless access systems (WiMAX) [5] have received particular attention since both IEEE 802.11 WLANs [7] and IEEE 802.16 WiMAX [8] operate in frequency bands that will be affected by first–generation UWB systems.

The performance degradation suffered by IEEE 802.11a WLANs as a result of generic impulse–radio (IR) UWB and direct sequence (DS) UWB interference was investigated by computer simulations in [3], [4]. While the simulative studies in [3], [4] are quite comprehensive, their applicability is limited to a particular victim BICM–OFDM system. Thus, it is difficult to deduce from these results qualitative or quantitative performance predictions for other existing or future BICM–OFDM systems using e.g. different OFDM sub–carrier spacings and/or different code rates. Analytical BER results are available for generic uncoded single–carrier systems impaired by generic IR–UWB [1], DS–UWB [9], and multi–band (MB) OFDM UWB [6]. Although these analytical results provide significant insights, their practical applicability is limited since

most existing and emerging wireless standards employ coded multi–carrier modulation in form of BICM–OFDM.

In this paper, we provide an analytical framework that allows us to accurately predict the bit error rate (BER) of a generic BICM–OFDM system impaired by UWB interference and additive white Gaussian noise (AWGN). For practical relevance, we concentrate on UWB formats that will be adopted in commercial products in the near future. In particular, we consider MB–OFDM, DS–UWB, and IR–UWB following the ECMA standard [10], the IEEE 802.15.3a standard proposal [11], and the IEEE 802.15.4a standard [12], respectively. We also derive a simple Gaussian approximation (GA) for the exact BER which is easy to compute. Our results show that the impact of UWB interference on BICM–OFDM strongly depends on the UWB format and on the OFDM sub–carrier spacing Δf_s . For example, while the GA is very accurate for DS–UWB and all sub–carrier spacings of practical interest (e.g. $\Delta f_s < 10$ MHz), for IR–UWB and MB–OFDM the GA is only accurate for $\Delta f_s < 100$ kHz. On the other hand, while the performance of the BICM–OFDM system is practically constant over the entire bandwidth of the IR–UWB and MB–OFDM systems, it is frequency–dependent for DS–UWB.

This paper is organized as follows. In Section II, the considered system model is presented, and in Section III the moment generating functions (MGFs) of the considered UWB formats are provided. The performance of BICM–OFDM in UWB interference is analyzed in Section IV. In Section V, this performance analysis is used to study the impact of the considered UWB formats on BICM–OFDM, and conclusions are drawn in Section VI.

Notations: In this paper, $[\cdot]^*$, $\mathcal{E}\{\cdot\}$, $\Re\{\cdot\}$, and \otimes denote complex conjugation, statistical expectation, the real part of a complex number, and convolution, respectively. In addition, a $\mathcal{N}(\mu, \sigma^2)$ distributed random variable is a Gaussian random variable with mean μ and variance σ^2 .

II. SYSTEM MODEL

The considered system model consists of one BICM–OFDM transmitter, one BICM–OFDM (victim) receiver, and I UWB interferers. We note that for convenience all signals and systems are represented by their complex baseband equivalents.

A. BICM–OFDM System

We assume that the victim system employs the popular BICM–OFDM concept, e.g. [13], [14]. Therefore, coding is performed along the frequency axis over the N_s sub–carriers of a single OFDM symbol using the concatenation of a

The completion of this research was made possible thanks to Bell Canada’s support through its Bell University Laboratories R&D program and the National Science and Engineering Research Council of Canada (Grant: STPGP 350451).

convolutional encoder of rate R_c , an interleaver, and a memoryless mapper. In particular, the elements of the codeword $\mathbf{c} \triangleq [c_1, c_2, \dots, c_{mN_s}]$ are interleaved, and the interleaved bits are broken up into sub-sequences of m bits each, which are subsequently mapped to symbols $x[k]$ from a constellation \mathcal{X} of size $|\mathcal{X}| \triangleq M = 2^m$ to form the transmit sequence $\mathbf{x} \triangleq [x[-N_s/2], x[-N_s/2+1], \dots, x[N_s/2-1]]$ (N_s is even). The transmit symbols $x[k]$ are modulated onto the N_s OFDM sub-carriers resulting in the baseband transmit signal

$$s(t) = \sum_{k=-\frac{N_s}{2}}^{\frac{N_s}{2}-1} x[k] \phi_k(t), \quad (1)$$

where $\phi_k(t) \triangleq e^{j2\pi\Delta f_s k t} w_s(t)$ is the k th OFDM sub-carrier waveform with sub-carrier spacing Δf_s . Here, $w_s(t)$ is a rectangular pulse with $w_s(t) = \sqrt{\Delta f_s}$, $-T_{\text{cp}} \leq t \leq 1/\Delta f_s$, and $w_s(t) = 0$ otherwise, where T_{cp} denotes the length of the cyclic prefix. The duration of the entire OFDM symbol is $T_s = T_{\text{cp}} + 1/\Delta f_s$.

$s(t)$ is transmitted over a multipath channel having impulse response $h(t)$ which is zero outside the interval $[0, T_{\text{cp}}]$. The received signal $r(t)$ is impaired by AWGN $n(t)$ and I UWB interferers $i_\nu(t)$, $1 \leq \nu \leq I$. Consequently, the received signal can be modeled as

$$r(t) = s(t) \otimes h(t) + n(t) + \sum_{\nu=1}^I g_\nu(t) \otimes e^{j2\pi f_\nu(t-\tau_\nu)} i_\nu(t-\tau_\nu) \quad (2)$$

where $g_\nu(t)$, τ_ν , and f_ν are the (causal) UWB interference channel impulse response (CIR) of length T_g , the delay, and the frequency offset of the ν th UWB signal, respectively. Both τ_ν and f_ν are defined relative to the center frequency of the victim signal. The typical OFDM receiver processing involving low-pass filtering, sampling, and discrete-time Fourier transform (DFT) can be equivalently represented by filtering of the received signal with a bank of matched filters $\psi_k(t) = \phi_k^*(-t)$, $-1/\Delta f_s \leq t \leq 0$, $-N_s/2 \leq k \leq N_s/2 - 1$, and $\psi_k(t) = 0$ otherwise, and subsequent sampling [15]. Assuming coherent reception, the sampled output of the k th, $-N_s/2 \leq k \leq N_s/2 - 1$, matched filter is obtained as

$$r[k] \triangleq e^{-j\Theta_H[k]} r(t) \otimes \psi_k(t)|_{t=0} = \alpha[k]x[k] + n[k] + i[k], \quad (3)$$

where $i[k]$ is the (effective) UWB interference, $H[k] \triangleq \int_0^{T_{\text{cp}}} h(t) e^{-j2\pi\Delta f_s k t} dt = \alpha[k] e^{j\Theta_H[k]}$ is the gain of the k th sub-carrier with magnitude $\alpha[k]$ and phase $\Theta_H[k]$, and $n[k]$ is AWGN. The UWB interference is given by

$$i[k] \approx \sum_{\nu=1}^I g_\nu[k] i_\nu[k], \quad (4)$$

where we have defined the discrete UWB interference channel $g_\nu[k]$ and the discrete UWB interference signal $i_\nu[k]$ of the ν th interferer as

$$g_\nu[k] \triangleq e^{-j\Theta_H[k]} e^{-j2\pi f_\nu \tau_\nu} G_\nu(k\Delta f_s), \quad (5)$$

$$i_\nu[k] \triangleq \psi_k(t) \otimes e^{j2\pi f_\nu t} i_\nu(t - \tau_\nu)|_{t=0}. \quad (6)$$

In deriving (4), we have assumed that the frequency response of the UWB channel $G_\nu(f) \triangleq \int_0^{T_g} g_\nu(t) e^{-j2\pi f t} dt$ is practically constant over the range of frequencies where $\psi_k(t)$ has significant energy.

Throughout this paper we assume that the $i_\nu[k]$, $g_\nu[k]$, and τ_ν are independent for different UWB interferers. Furthermore, as customary in the literature [14], we assume that the $H[k]$ are independent and identically distributed (i.i.d.) $\mathcal{N}(0, 1)$ RVs, where the independence is due to the bit-interleaving which is assumed to be ideal. This follows that the $\alpha[k]$ are i.i.d. Rayleigh distributed RVs. The delays τ_ν are modelled as uniformly distributed in $[0, T_s)$.

Finally, we assume that the UWB interference channel $g_\nu(t)$ is constant. This follows that the discrete UWB interference channel $g_\nu[k]$ can be modelled as $g_\nu[k] = \bar{g}_\nu e^{j\Theta_\nu[k]}$, cf. (5), where $\bar{g}_\nu \triangleq |g_\nu[k]|$ is constant and $\Theta_\nu[k]$ is uniformly distributed in $[-\pi, \pi)$. We note that the phase of $H[k]$ renders $\Theta_\nu[k]$ and consequently $g_\nu[k]$ i.i.d. for different k . Assuming a constant interference channel corresponds to the AWGN assumption for the interference channel and is popular in the literature, e.g. [16], [17], as it allows an unobscured view of the degradation caused by the interference signal.

B. UWB Signal Model

In this paper, we consider MB-OFDM [10], DS-UWB [11], and IR-UWB [12] for the interference signal. We note that the three underlying standards/standard proposals [10], [11], [12] also include optional forward error correction (FEC) coding. However, since the applied FEC coding does not change the relevant statistical properties of the UWB transmit symbols, it can be ignored for the purpose of interference analysis. For simplicity of notation, we drop the subscript ν in the UWB signal $i_\nu(t)$ in the following if no confusion arises. We will keep our discussion of MB-OFDM and DS-UWB very short since these interference formats have already been discussed in [6], [9], and provide more details about the adopted IR-UWB signal model.

1) *MB-OFDM Signal Model*: The adopted MB-OFDM model closely follows the ECMA standard [10]. MB-OFDM is a standard OFDM system ($N_i = 128$ sub-carriers and $\Delta f_i = 4.125$ MHz sub-carrier spacing) with additional frequency hopping over 3 bands. For a detailed discussion of MB-OFDM interference we refer to [6].

2) *DS-UWB Signal Model*: For DS-UWB we closely follow the IEEE 802.15.3a standard proposal [11], where both binary phase-shift keying (BPSK) and 4-ary bi-orthogonal keying (4-BOK) are considered for modulation. The standard proposal [11] envisions two frequency bands of operation: a lower band from 3.1 GHz to 4.85 GHz and a higher band from 6.2 GHz to 9.7 GHz. Here, we concentrate on the lower operating band with a chip duration of $T_c = 0.762$ ns and a bandwidth of $B_s = 1.3$ GHz. The data rate of DS-UWB is adjusted via the spreading sequence length which varies between $L = 1$ and $L = 24$, cf. [11, Tables 3–6]. We note that the power spectral density (PSD) of DS-UWB is flat for $L < 12$ since in that case the spreading sequences have only

a single non-zero chip. However, for $L = 12$ and $L = 24$ the PSD is not flat since there are multiple non-zero chips. For more details on DS-UWB we refer to [11], [9].

3) *IR-UWB Signal Model*: For IR-UWB we adopt the signal model proposed by the IEEE 802.15.4a standardization committee [12] which employs a combination of BPSK and binary pulse position modulation (BPPM). An IR-UWB symbol has duration T_i and consist of N_b bursts of duration $T_b = T_i/N_b$. Similarly, a burst consist of L chips of duration $T_c = T_b/L$. The IR-UWB signal can be modeled as

$$i(t) = \sum_{\kappa=-\infty}^{\infty} \sum_{l=0}^{L-1} a[\kappa] p[\kappa, l] p_c(t - \kappa T_i - h[\kappa] T_b - l T_c - b[\kappa] T_{\text{PPM}}) \quad (7)$$

where $a[\kappa] \in \{\pm 1\}$ and $b[\kappa] \in \{0, 1\}$ denote the i.i.d. BPSK and BPPM data symbols, respectively. Furthermore, $p_c(t)$ is the root-raised cosine chip waveform with roll-off factor 0.6 and T_{PPM} is the delay for BPPM. $p[\kappa, l] \in \{\pm 1\}$ and $h[\kappa] \in \{0, 1, \dots, N_h - 1\}$ are the i.i.d. scrambling sequence and the i.i.d. hopping sequence, respectively, where N_h denotes the number of hopping positions.

Similar to DS-UWB, IR-UWB has a lower operating band from 3.2 GHz to 4.7 GHz and a higher operating band from 5.9 GHz to 10.3 GHz. The only mandatory data rate is 0.811 Mb/s in the lower operating band, but in both bands there are several optional data rates ranging from 0.1 Mb/s to 26.03 Mb/s. N_b , L , and T_{PPM} depend on the data rate and are specified in [12, Table 38a].

III. MGF OF UWB INTERFERENCE SIGNAL

For the error rate analysis presented in Section IV the MGF $\Phi_{i_\nu[k]}(s|g_\nu[k], \tau_\nu) \triangleq \mathcal{E}\{e^{-s \Re\{g_\nu[k] i_\nu[k]\}} | g_\nu[k], \tau_\nu\}$ of $\Re\{g_\nu[k] i_\nu[k]\}$ conditioned on $g_\nu[k]$ and τ_ν plays a major role. For simplicity of notation we drop the index ν in the remainder of this section.

For calculation of the interference MGF of IR-UWB it is convenient to rewrite (7) as

$$i(t) = \sum_{\kappa=-\infty}^{\infty} \sum_{l=0}^{L-1} \tilde{a}[\kappa, l] p_c(t - \kappa T_i - l T_c - \vartheta[\kappa]), \quad (8)$$

where $\tilde{a}[\kappa, l] \triangleq a[\kappa] p[\kappa, l]$ and $\vartheta[\kappa] \triangleq h[\kappa] T_b + b[\kappa] T_{\text{PPM}}$. We note that $\tilde{a}[\kappa, l] \in \{\pm 1\}$ is i.i.d. and $\vartheta[\kappa]$ is i.i.d. and has pdf

$$p_\vartheta(\vartheta) = \frac{1}{2N_h} \sum_{h=0}^{N_h-1} \sum_{b=0}^1 \delta(\vartheta - h T_b - b T_{\text{PPM}}). \quad (9)$$

From (6) we obtain for the discrete UWB interference signal

$$\begin{aligned} i[k] &= \sqrt{\Delta f_s} \int_0^{1/\Delta f_s} e^{j2\pi(f - \Delta f_s k)t} i(t - \tau) dt \\ &= \sum_{\kappa=-\infty}^{\infty} \sum_{l=0}^{L-1} \tilde{a}[\kappa, l] \beta_l[\kappa, k, \vartheta[\kappa]], \end{aligned} \quad (10)$$

where

$$\begin{aligned} \beta_l[\kappa, k, \vartheta[\kappa]] &= \sqrt{\Delta f_s} e^{j2\pi(f - \Delta f_s k)(\tau + \kappa T_i + l T_c + \vartheta[\kappa])} \\ &\quad \cdot \int_{l_i}^{l_u} e^{j2\pi(f - \Delta f_s k)t} p_c(t) dt \end{aligned} \quad (11)$$

with limits $l_u = 1/\Delta f_s - \tau - \kappa T_i - l T_c - \vartheta[\kappa]$ and $l_l = -\tau - \kappa T_i - l T_c - \vartheta[\kappa]$. Using $i[k]$ from (10) and averaging over $\tilde{a}[\kappa, l]$, which is i.i.d. with respect to both κ and l , we obtain

$$\Phi_{i[k]}(s|g[k], \tau, \vartheta[\kappa]) = \prod_{\kappa=-\infty}^{\infty} \prod_{l=0}^{L-1} \cosh(s \Re\{g[k] \beta_l[\kappa, k, \vartheta[\kappa]]\}). \quad (12)$$

Exploiting that $\vartheta[\kappa]$ is an i.i.d. RV and averaging $\Phi_{i[k]}(s|g[k], \tau, \vartheta[\kappa])$ with respect to $\vartheta[\kappa]$ yields

$$\begin{aligned} \Phi_{i[k]}(s|g[k], \tau) &\simeq \\ &\prod_{\kappa=-\infty}^{\infty} \frac{1}{2N_h} \sum_{h=0}^{N_h-1} \sum_{b=0}^1 \prod_{l=0}^{L-1} \cosh(s \Re\{g[k] \beta_l[\kappa, k, h T_b + b T_{\text{PPM}}]\}) \end{aligned} \quad (13)$$

For calculation of $\Phi_{i[k]}(s|g[k], \tau)$ the infinite limits of the product in (13) can be truncated to finite values and the integral in (11) can be evaluated using standard numerical techniques.

For MB-OFDM and DS-UWB the results for single-carrier victim systems provided in [9], [6] can be exploited for calculation of $\Phi_{i[k]}(s|g[k], \tau)$. In particular, $\Phi_{i_\nu[k]}(s|g_\nu[k], \tau_\nu)$ for the k th sub-carrier can be essentially obtained by replacing the receiver input filter in [9], [6] with $\psi_k(t)$. Because of space limitation, we cannot provide further details here.

IV. BER OF BICM-OFDM SYSTEMS

In this section, we derive a tight upper bound on the exact BER of a BICM-OFDM victim receiver impaired by UWB interference and AWGN. In addition, we also provide a simple and easy-to-evaluate GA for this upper bound. However, first we briefly review the bit metric used for Viterbi decoding in the BICM-OFDM receiver and calculate the conditional MGF of the metric difference.

A. Conditional MGF of Metric Difference

As customary, we assume that the BICM-OFDM system employs Viterbi decoding with branch metric [13]

$$\lambda_i[k] \triangleq \min_{x[k] \in \mathcal{X}_b^i} \{|r[k] - \alpha[k] x[k]|^2\} \quad (14)$$

for the i th bit of the k th sub-carrier. Here, \mathcal{X}_b^i denotes that subset of all symbols in constellation \mathcal{X} the labels of which have value $b \in \{0, 1\}$ in position i . For BER calculation the MGF of the metric difference

$$\begin{aligned} \Delta(x[k], z[k]) &\triangleq |r[k] - \alpha[k] x[k]|^2 - |r[k] - \alpha[k] z[k]|^2 \\ &= -\alpha^2[k] d_{xz}^2[k] + 2\alpha[k] d_{xz}[k] \Re\{e^{-j\Theta_d[k]}(i[k] + n[k])\} \end{aligned} \quad (15)$$

is of interest, where $x[k]$ and $z[k] \neq x[k]$ denote the transmitted symbol and another symbol in \mathcal{X} , respectively. Furthermore, we used in (15) the definition $x[k] - z[k] \triangleq$

$d_{xz}[k]e^{j\Theta_d[k]}$, where $d_{xz}[k]$ and $\Theta_d[k]$ denote the magnitude and phase, respectively. Since both $i[k]$ and $n[k]$ are rotationally symmetric RVs, cf. Section II, we can express the conditional MGF of $\Delta(x[k], z[k])$ as

$$\Phi_{\Delta(x[k], z[k])}(s|\mathbf{g}[k], \boldsymbol{\tau}, \alpha[k]) \triangleq \mathcal{E} \left\{ e^{-s\Delta(x[k], z[k])} \right\} \quad (16)$$

$$= e^{\alpha^2[k]d_{xz}^2[k](1+s\sigma_n^2)s} \prod_{\nu=1}^I \Phi_{i_\nu[k]}(2\alpha[k]d_{xz}[k]s|g_\nu[k], \tau_\nu),$$

where we used the definitions $\mathbf{g}[k] \triangleq [g_1[k] \dots g_I[k]]$ and $\boldsymbol{\tau} \triangleq [\tau_1 \dots \tau_I]$, the fact that $n[k]$ is $\mathcal{N}(0, \sigma_n^2)$ distributed with MGF $\Phi_n(s) = \mathcal{E}\{e^{-sn[k]}\} = e^{s^2\sigma_n^2}$, and the assumption that the UWB interferers are mutually independent.

B. Union Bound for BER

The union bound for the BER of a convolutional code (CC) of rate $R_c = k_c/n_c$ (k_c and n_c are integers) is given by

$$P_b \leq \frac{1}{k_c} \sum_{d=d_{\min}}^{\infty} w_c(d) P(\mathbf{c} \rightarrow \hat{\mathbf{c}}), \quad (17)$$

where \mathbf{c} and $\hat{\mathbf{c}}$ are two distinct code sequences with Hamming distance d that differ only in $l \geq 1$ consecutive trellis states. Furthermore, $w_c(d)$ and d_{\min} denote the total input weight of error events at Hamming distance d and the minimum Hamming distance of the code, respectively. $P(\mathbf{c} \rightarrow \hat{\mathbf{c}})$ is the pairwise error probability (PEP), i.e., the probability that the decoder erroneously chooses the code sequence $\hat{\mathbf{c}}$ when the code sequence \mathbf{c} is transmitted. It is convenient to express the PEP in terms of an MGF as [13]

$$P(\mathbf{c} \rightarrow \hat{\mathbf{c}}) = \frac{1}{2\pi j} \int_{c-j\infty}^{c+j\infty} \mathcal{E}_\tau \{ \Psi(s|\boldsymbol{\tau}) \} \frac{ds}{s}, \quad (18)$$

where c is a small positive constant that lies in the region of convergence of the integral. The MGF $\Psi(s|\boldsymbol{\tau})$ is conditioned on $\boldsymbol{\tau}$ since the delay $\boldsymbol{\tau}$ is constant for one OFDM symbol, and thus the bit de-interleaving does not result in an averaging with respect to $\boldsymbol{\tau}$. Following the same steps as in [13] for the AWGN channel and exploiting (16), we obtain $\Psi(s|\boldsymbol{\tau}) = (\tilde{\Psi}(s|\boldsymbol{\tau}))^d$ with

$$\tilde{\Psi}(s|\boldsymbol{\tau}) = \frac{1}{m2^m N_s} \sum_{k=-\frac{N_s}{2}}^{\frac{N_s}{2}-1} \sum_{i=1}^m \sum_{b=0}^1 \sum_{x[k] \in \mathcal{X}_b^i} \quad (19)$$

$$\mathcal{E}_\alpha \left\{ e^{\alpha^2 d_{xz}^2[k](1+s\sigma_n^2)s} \prod_{\nu=1}^I \mathcal{E}_{g_\nu} \{ \Phi_{i_\nu[k]}(2\alpha d_{xz}[k]s|g_\nu, \tau_\nu) \} \right\},$$

where $z[k]$ represents the nearest neighbor of $x[k]$ in \mathcal{X}_b^i with \bar{b} being the bit complement of b , i.e., we invoke the BICM expurgated bound from [13].

An approximate upper bound for the BER of a BICM-OFDM victim receiver impaired by UWB interference and noise can be obtained by truncating the union bound in (17) and using (18) in combination with (16) and (19). Thereby, the integral in (18) can be efficiently evaluated using a Gauss-Chebyshev quadrature rule, cf. [18] for details.

C. Gaussian Approximation

If the UWB interference signals $i_\nu[k]$ are modeled as $\mathcal{N}(0, \sigma_{i_\nu}^2[k])$ distributed with $\sigma_{i_\nu}^2[k] \triangleq \mathcal{E}\{i_\nu[k]^2\}$, the variance of $n[k] + i[k]$ conditioned on $g_\nu[k]$ is given by $\sigma^2[k] = \sigma_n^2 + \sum_{\nu=1}^I |g_\nu[k]|^2 \sigma_{i_\nu}^2[k]$. In this case, the PEP in (18) can be simplified to

$$P(\mathbf{c} \rightarrow \hat{\mathbf{c}}) = \frac{1}{2\pi j} \int_{c-j\infty}^{c+j\infty} (\tilde{\Psi}(s))^d \frac{ds}{s} \quad (20)$$

$$\tilde{\Psi}(s) = \frac{1}{m2^m N_s} \sum_{k=-\frac{N_s}{2}}^{\frac{N_s}{2}-1} \sum_{i=1}^m \sum_{b=0}^1 \sum_{x[k] \in \mathcal{X}_b^i} \tilde{\Psi}(s|d_{xz}[k]) \quad (21)$$

where

$$\tilde{\Psi}(s|d_{xz}[k]) = \frac{1}{1 + s d_{xz}^2[k] [1 + s(\sigma_n^2 + \sum_{\nu=1}^I \bar{g}_\nu^2 \sigma_{i_\nu}^2[k])]} \quad (22)$$

An approximation for the BER of a BICM-OFDM receiver can be obtained by combining (17) and (20)–(22). The integral in (20) can again be efficiently evaluated using a Gauss-Chebyshev quadrature rule.

V. RESULTS AND DISCUSSION

In this section, after verifying the validity of our results in Section IV with computer simulations in Subsection V-B, we use these analytical results to highlight the effects of the considered UWB formats on a BICM-OFDM system in Subsection V-C. However, first we specify the system parameters used for the simulations and numerical evaluations.

A. System Parameters

Throughout this section we consider a BICM-OFDM system with $N_s = 64$ sub-carriers. We found however that the performance is almost independent of N_s for $N_s \geq 16$ which will be true for most practical systems. For BICM we assumed ideal interleaving and we adopted the rate 1/2 quasi-standard code with generator polynomials [133, 171] (octal representation), which is used e.g. in both IEEE 802.11a WLANs [7] and IEEE 802.16 WiMAX [8]. Higher code rates were obtained via puncturing using the puncturing patterns from [7]. For simplicity, we consider the case of a single UWB interferer, i.e., $I = 1$.

In the following, the terms SNR and SIR refer to the SNR and SIR per information bit. Unless stated otherwise, puncturing is not applied, the frequency offset is set to $f_1 = 8.25$ MHz and 4-PSK modulation is used. The various parameters for the UWB signals were taken from [10]–[12].

B. Verification of Theoretical Results

In Fig. 1 we show the BER vs. SIR for MB-OFDM, BPSK DS-UWB ($L = 24$), and IR-UWB ($N_b = 32$, $L = 16$) interference for different BICM-OFDM sub-carrier spacings Δf_s . An interference limited scenario is considered (i.e., $\text{SNR} \rightarrow \infty$). Fig. 1 includes simulation results, theoretical results obtained by evaluating the analytical expressions in

Section IV, and the GA. For the theoretical results the union bound in (17) is truncated after the first 8 terms. As can be observed from Fig. 1 for relevant BERs (e.g. $\text{BER} \leq 10^{-4}$), where the union bound becomes tight, the theoretical results are in perfect agreement with the simulations for all considered UWB formats and sub-carrier spacings. We note that although the analytical BER expressions involve integrals, which have to be evaluated numerically, it took only minutes to compute the theoretical BER curves in Fig. 1. In contrast, the simulations for Fig. 1 took several days to finish¹.

We observe from Fig. 1 that the BER strongly depends on the UWB interference format and the sub-carrier spacing. The GA is only a good approximation for DS-UWB. However, it is interesting to note that all BER curves have the same asymptotic slope as the GA.

Having confirmed the accuracy of the derived analytical results, we will use these results in the following subsection to investigate the influence of the UWB format on BICM-OFDM performance.

C. Effect of UWB Format

Since the effects of all BICM-OFDM and UWB parameters on the BER crucially depend on the BICM-OFDM sub-carrier spacing Δf_s , we show in this subsection the BER as a function of Δf_s . In this context, it might be helpful to note that the sub-carrier spacings for IEEE 802.11a WLANs [7] and IEEE 802.16 WiMAX [8] are $\Delta f_s = 312.5$ kHz and $\Delta f_s \leq 89.3$ kHz, respectively. However, our results are not limited to narrowband BICM-OFDM systems and can also be used to evaluate the impact of UWB interference on wideband or UWB BICM-OFDM systems. An example for the latter case is the MB-OFDM UWB system [10] which also uses the BICM-OFDM concept and has a sub-carrier spacing of 4.125 MHz.

In Figs. 2 and 3 we investigate the impact of the UWB format on the BER and the validity of the GA for $\text{SNR} = 15$ dB and $\text{SIR} = 10$ dB. Fig. 2 shows that for IR-UWB the validity of the GA strongly depends Δf_s and on the data rate of the IR-UWB system. For the lowest data rate of 0.1 MHz (corresponding to $L = 32$ and $L = 128$, respectively) IR-UWB is highly impulsive and the GA is not accurate in the considered Δf_s range. Similarly, for the mandatory data rate of 0.811 MHz ($L = 16$) in the lower frequency band the GA leads to overly optimistic performance predictions for $\Delta f_s \geq 100$ kHz. For example, for the sub-carrier spacing used in IEEE 802.11a WLANs the GA suggests that the BER is approximately by a factor of 1.5 lower than it actually is. For very high IR-UWB data rates ($L = 1$) the GA is fairly accurate in the considered Δf_s range since the IR-UWB data signal is less impulsive in this case. Fig. 3 shows that the GA is very accurate for BPSK and 4-BOK DS-UWB. We note that we only show results for the lower operating

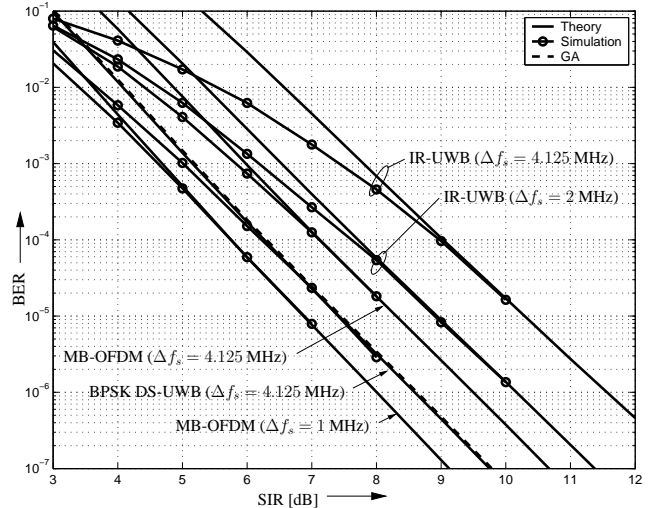


Fig. 1. BER vs. SIR for IR-UWB ($N_b = 32$, $L = 16$), BPSK DS-UWB ($L = 24$), and MB-OFDM, $\text{SNR} \rightarrow \infty$, and $R_c = 1/2$.

band and $L = 24$ (corresponding to the lowest DS-UWB data rates). However, the results for smaller L (corresponding to higher data rates) and the higher operating band are very similar and are also in excellent agreement with the GA. For MB-OFDM interference the GA may over- or underestimate the performance depending on Δf_s and is accurate only for $\Delta f_s \leq 100$ kHz. For the sub-carrier spacing of IEEE 802.11a WLANs the GA leads to slightly too pessimistic performance predictions. On the other hand, if one MB-OFDM system is impaired by another, interfering MB-OFDM system, the GA underestimates the true BER by a factor of 4. Finally, we note that for the relatively small sub-carrier spacings used in IEEE 802.16 WiMAX the GA is very accurate for MB-OFDM, DS-UWB, and IR-UWB with $L \geq 16$ corresponding to data rates of 0.811 MHz or more.

Accuracy of the GA: For system-level simulations a simple interference model is desirable and it is convenient if UWB interference can be modeled as additional AWGN. Figs. 2 and 3, and additional results not shown here because of space limitation allow us to draw some general conclusions regarding the GA for the UWB interference. These conclusions are practically independent of the modulation scheme, the code rate, and the channel of the BICM-OFDM system. First, we note that the GA is very accurate for DS-UWB in the entire range of relevant sub-carrier spacings (e.g. $\Delta f_s \leq 10$ MHz). On the other hand, for IR-UWB operating with the mandatory data rate of 0.811 Mb/s the GA underestimates the BER of the BICM-OFDM system and becomes tight only for $\Delta f_s \leq 100$ kHz. For MB-OFDM the GA overestimates the BER for $\Delta f_s < 2$ MHz but underestimates it for $\Delta f_s > 2$ MHz. The GA becomes tight again for $\Delta f_s \leq 100$ kHz.

VI. CONCLUSIONS

In this paper, we have provided an analytical performance evaluation framework for generic BICM-OFDM systems impaired by UWB interference. The considered UWB formats

¹Both the simulations and numerical evaluations were performed on the same computer (with two Intel Xeon 3.6 GHz processors). The simulation program was written in C, whereas MATLAB was used for the numerical evaluations.

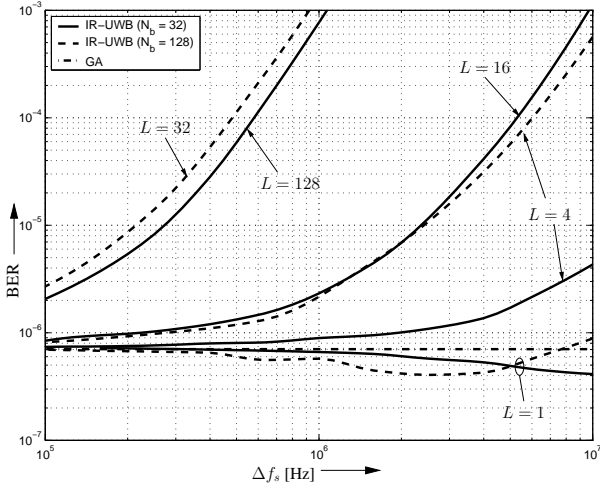


Fig. 2. BER vs. Δf_s for IR-UWB with different N_b and L , SNR = 15 dB, SIR = 10 dB, and $R_c = 1/2$.

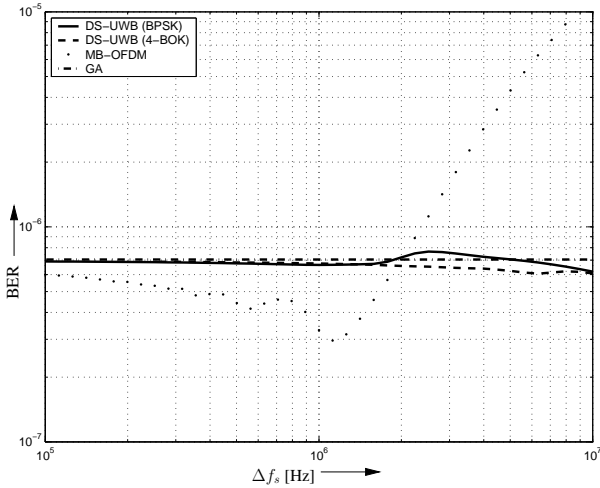


Fig. 3. BER vs. Δf_s for BPSK DS-UWB ($L = 24$), 4-BOK DS-UWB ($L = 24$), and MB-OFDM, SNR = 15 dB, SIR = 10 dB, and $R_c = 1/2$.

closely follow IEEE/ECMA standards or standard proposals. Besides the accurate analysis we have also proposed a simple GA where the UWB interference is treated as additional AWGN. Our results show that while for DS-UWB the GA is applicable for all practically relevant BICM-OFDM sub-carrier spacings (e.g. $\Delta f_s < 10$ MHz), for MB-OFDM and IR-UWB the GA becomes tight only for $\Delta f_s < 100$ kHz. For larger sub-carrier spacings the GA may severely underestimate the BER for IR-UWB interference employing the mandatory data rate of 0.811 Mb/s. In contrast, for MB-OFDM the GA underestimates the BER for $\Delta f_s < 2$ MHz but overestimates it for $\Delta f_s > 2$ MHz. For example, for IEEE 802.11a WLANs the GA overestimates the BER for MB-OFDM interference but underestimates it for IR-UWB interference. In contrast, if an MB-OFDM system is interfered by other UWB systems, the GA underestimates the BER for both IR-UWB and MB-OFDM interference.

In summary, the presented results give important insights into the impact of various UWB interference formats on the

performance of BICM-OFDM systems and shed new light on the validity of the popular GA.

REFERENCES

- [1] J.R. Foerster. Interference Modeling of Pulse-based UWB Waveforms on Narrowband Systems. In *Proceedings of IEEE Vehicular Technology Conference (VTC)*, pages 1931–1935, Birmingham, AL., May 2002.
- [2] M. Hämäläinen, V. Hovinen, R. Tesi, J. Iinatti, and M. Latva-aho. On the UWB System Coexistence With GSM900, UMTS/WCDMA, and GPS. *IEEE J. Select. Areas Commun.*, 20:1712–1721, December 2002.
- [3] J. Bellorado, S. Ghassemzadeh, L. Greenstein, T. Sveinsson, and V. Tarokh. Coexistence of Ultra-Wideband Systems with IEEE-802.11 a Wireless LANs. In *Proceedings of the IEEE Global Telecommun. Conf. (Globecom)*, pages 410–414, November 2003.
- [4] D. Borah, R. Jana, and A. Stamoulis. Performance Evaluation of IEEE 802.11a Wireless LANs in the Presence of Ultra-Wideband Interference. In *Proceedings of the IEEE Wireless Commun. and Networking Conf. (WCNC)*, pages 83–87, March 2003.
- [5] R. Giuliano and F. Mazzenga. On the Coexistence of Power Controlled Ultrawide-Band Systems with UMTS, GPS, DCS1800, and Fixed Wireless Systems. *IEEE Trans. Veh. Technol.*, VT-54:62–81, January 2005.
- [6] A. Nasri, R. Schober, and L. Lampe. Analysis of Narrowband Communication Systems Impaired by MB-OFDM UWB Interference. To appear in *IEEE Transactions on Wireless Communication [Online]* <http://www.ece.ubc.ca/amir/MBOFDM.pdf>, 2007.
- [7] IEEE 802.11a Standard. Part 11: Wireless LAN Medium Access Control (MAC) and Physical Layer (PHY) specifications.
- [8] IEEE 802.16 Standard. IEEE Standard for Local and Metropolitan Area Networks Part 16: Air Interface for Fixed Broadband Wireless Access Systems.
- [9] A. Nasri, R. Schober, and L. Lampe. Comparison of MB-OFDM and DS-UWB Interference. In *Proceedings of the IEEE Intern. Conf. on Ultra-Wideband (ICUWB)*, pages 489–494, September 2006.
- [10] ECMA. Standard ECMA-368: High Rate Ultra Wideband PHY and MAC Standard. [Online] <http://www.ecma-international.org/publications/standards/Ecma-368.htm>, December 2005.
- [11] IEEE P802.15. DS-UWB Physical Layer Submission to IEEE 802.15 Task Group 3a (Doc. Number P802.15-04/0137r4). January 2005.
- [12] IEEE P802.15.4a. Part 15.4: Wireless Medium Access Control (MAC) and Physical Layer (PHY) Specifications for Low-Rate Wireless Personal Area Networks (LR-WPANs): Amendment to Add Alternate PHY. January 2007.
- [13] Giuseppe Caire, Giorgio Taricco, and Ezio Biglieri. Bit-Interleaved Coded Modulation. *IEEE Trans. Inform. Theory*, 44:927–946, May 1998.
- [14] E. Akay and E. Ayanoglu. Achieving Full Frequency and Space Diversity in Wireless Systems via BICM, OFDM, STBC, and Viterbi Decoding. *IEEE Trans. Commun.*, 54:2164–2172, December 2006.
- [15] O. Edfors, M. Sandell, J. van de Beek, D. Landström, and F. Sjöberg. An Introduction to Orthogonal Frequency-Division Multiplexing. 2005. [Online]: <http://www.sm.luth.se/csee/sp/research/report/esb96rc.pdf>.
- [16] B. Hu and N. Beaulieu. Accurate Performance Evaluation of Time-Hopping and Direct-Sequence UWB Systems in Multi-User Interference. *IEEE Trans. Commun.*, 54:1053–1062, June 2005.
- [17] N. Kokkalis, P. Mathiopoulos, G. Karagiannidis, and C. Koukourlis. Performance Analysis of M -ary PPM TH-UWB Systems in the Presence of MUI and Timing Jitter. *IEEE J. Select. Areas Commun.*, 24:822–828, April 2006.
- [18] E. Biglieri, G. Caire, G. Taricco, and J. Ventura-Traveset. Computing Error Probabilities over Fading Channels: a Unified Approach. *European Transactions on Telecommunications*, 9:15–25, January-February 1998.